This is a preproof accepted article for *Mineralogical Magazine* This version may be subject to change during the production process DOI: 10.1180/mgm.2025.10157

# Metaheimite, PbCu<sub>2</sub>(AsO<sub>4</sub>)(OH)<sub>3</sub>, a new mineral with [4+1]-coordinated Cu<sup>2+</sup>

Thomas Malcherek<sup>1\*</sup>, Boriana Mihailova<sup>1</sup>, Jochen Schlüter<sup>2</sup>, Philippe Roth<sup>3</sup>, Nicolas Meisser<sup>4</sup>

#### Abstract

Metaheimite (IMA 2023-020a), PbCu<sub>2</sub>(AsO<sub>4</sub>)(OH)<sub>3</sub>, has been identified as a new secondary mineral at the Grosses Chalttal deposit, Mürtschenalp district, Glarus, Switzerland. It forms radial aggregates of blade-like crystals of light blue to turquoise blue colour. Metaheimite has a light blue streak and vitreous to silky lustre. Its calculated density is 5.47 g cm<sup>-3</sup>. The empirical chemical formula based on seven anions per formula unit is (Pb<sub>0.96</sub>Ca<sub>0.03</sub>)Cu<sub>1.98</sub>(As<sub>1.01</sub>O<sub>4</sub>)(OH)<sub>3</sub>. Metaheimite is pseudo-orthorhombic, with monoclinic symmetry, space group  $P2_1/n$  and unit cell parameters a = 5.8347(4), b = 7.7528(6), c = $13.8899(9) \text{ Å}, \beta = 90.018(3)^{\circ}, V = 628.31(8) \text{ Å}^3 \text{ and } Z = 4.$  The five strongest lines in the calculated powder diffraction pattern are (d in Å(I)hkl) as follows: 6.945(100)002, 3.870(75)112, 3.169(78)014, 3.145(99)121, 2.615(81)015. The crystal structure, refined to  $R_{obs}$ =6.13% for 1393 reflections with  $I > 3\sigma(I)$ , consists of layers similar to those occurring in heimite, PbCu<sub>2</sub>(AsO<sub>4</sub>)(OH)<sub>3</sub>·2H<sub>2</sub>O, but with 6+2 coordinated Pb<sup>2+</sup>. The lack of water molecules in metaheimite causes different interlayer hydrogen bonding and consequently, different layer stacking order as compared to that in heimite. In metaheimite, Cu<sup>2+</sup> therefore occurs in a square-pyramidal coordination by five oxygen atoms. Hydrous species in metaheimite have been examined by Raman- and by infrared spectroscopy. Metaheimite is structurally related to duftite, PbCu(AsO<sub>4</sub>)(OH) and may be considered a transitional state between heimite and duftite.

**Keywords:** metaheimite; new mineral; heimite; Cu-coordination; arsenic; hydrous species; duftite

<sup>&</sup>lt;sup>1</sup> Mineralogisch-Petrographisches Institut, Fachbereich Erdsystemwissenschaften, Universität Hamburg, Grindelallee 48, D-20146 Hamburg, Germany

<sup>&</sup>lt;sup>2</sup> Mineralogisches Museum Hamburg, Grindelallee 48, D-20146 Hamburg, Germany

<sup>&</sup>lt;sup>3</sup> Swiss Seismological Service, ETH Zürich, Sonneggstr. 5, CH-8092 Zurich, Switzerland

<sup>&</sup>lt;sup>4</sup> Muséum cantonal des sciences naturelles (Naturéum), Département de géologie, Université de Lausanne, Anthropole, Dorigny, CH-1015 Lausanne, Switzerland

<sup>\*</sup>E-mail: thomas.malcherek@uni-hamburg.de

## Introduction

The recently discovered mineral heimite, PbCu<sub>2</sub>(AsO<sub>4</sub>)(OH)<sub>3</sub> • 2H<sub>2</sub>O, has been suggested to form as a metastable precursor of duftite, PbCu(AsO<sub>4</sub>)(OH) (Malcherek et al., 2024). In addition to its type locality at the Grosses Chalttal deposit and other localities in the Swiss Alps (Malcherek et al., 2024), heimite has also been reported from the Laurion mining district, Greece (Branko Rieck, personal communication). Zanelliite, PbCu<sub>9</sub>[AsO<sub>3.5</sub>(OH)<sub>0.5</sub>]<sub>2</sub>(AsO<sub>4</sub>)<sub>2</sub>(OH)<sub>9</sub> (H<sub>2</sub>O)<sub>3</sub> (Biagioni et al. 2024), is another new hydrous lead-copper-arsenate that occurs in association with heimite at the Grosses Chalttal deposit.

It was previously conjectured that the partial dehydration of heimite would inevitably lead to some of the  $Cu^{2+}$  cations in the heimite structure to become 5-fold coordinated by oxygen atoms (Malcherek et al., 2024). The new mineral presented here is a derivative of heimite, in which the  $Cu^{2+}$  ion is exclusively [4+1] coordinated, owing to the complete absence of molecular  $H_2O$ . The layered crystal structure of metaheimite differs from the heimite structure by a relative shift of layers otherwise similar to those occurring in the heimite crystal structure.

The name metaheimite recognizes its similarity to heimite as well as the lack of water molecules coordinating the Cu-cations. The new mineral, its name and abbreviation, Mhim, have been approved by the International Mineralogical Association (IMA 2023-020a, Malcherek et al. 2025) and the holotype is deposited at the Museum der Natur Hamburg – Mineralogie, Leibniz-Institut zur Analyse des Biodiversitätswandels (LIB), Grindelallee 48, 20146 Hamburg, Germany, catalog number ro-3702. Author-collected and studied samples of metaheimite and its associated mineral paragenesis are housed at the Département de géologie of Muséum cantonal des sciences naturelles (Naturéum), UNIL, 1015-Lausanne, Switzerland, catalogue numbers MGL 087051 to 087057.

## **Occurrence**

As was the case with heimite, metaheimite was discovered on the dump of the Grosses Chalttal deposit, Mürtschenalp district, Glarus, Switzerland (47°04'09.9", 9°11'26.5", E). The Grosses Chalttal deposit, like all the mines and small deposits that make up the Mürtschenalp district (Bächtiger, 1963), is located in the Helvetic nappes of eastern

Switzerland, within the up to 1000 m thick Permian Verrucano formation, which consists of layered volcanic rocks, sandstones and conglomerates. During Oligocene—Miocene times, the Verrucano was pushed northwards at least 40 km along the famous Glarus Thrust above younger Cretaceous carbonates and Tertiary Flysh sediments (Badertscher *et al.*, 2001; Pfiffner, 2014). At Grosses Chalttal, the rock appears in its coarse fanglomeratic *Sernifite facies* (Letsch *et al.*, 2014), as a pale grey to greenish breccia.

The Grosses Chalttal Cu and partly U mineralization has a sedimentary origin with at least two phases of later remobilization (Bächtiger, 1963). The primary ore assemblage is made mainly of bornite, tennantite and the uraninite variety pitchblende. A broad suite of secondary minerals, primarily arsenates and sulfates, with only rare carbonates, has been described (Meisser, 1999; Roth et al., 2025). Noteworthy is the presence of the rare Cu-arsenate euchroite. Malachite, brochantite, tyrolite, mimetite and chrysocolla are mineral species commonly associated with metaheimite. Because of the discovery of the type material in form of a small sample on the mine dumps, a contextualization of the occurrence of the new mineral species in the ore body is not possible.

## Appearance and physical properties

Metaheimite occurs as radial aggregates of up to 500  $\mu$ m radius, composed of light blue to blue or turquoise blue, blade like crystals (Figure 1 and 2). Single-crystal X-ray diffraction (XRD) analysis showed that metaheimite exhibits monoclinic symmetry and that the crystals are elongated along [100] and flattened normal to (001). Individual crystals measure up to 200  $\mu$ m in length and 20  $\mu$ m in width, with {001}, {100} and {010} being most prominent (Figure 2).

Metaheimite exhibits a light blue streak and vitreous to silky lustre. Due to the small size and the extreme brittleness of the crystals no Mohs- or micro-indentation hardness could be determined. Fluorescence was not observed. Crystals of metaheimite show perfect cleavage on  $\{001\}$  and uneven fracture. The calculated density is 5.47 g cm<sup>-3</sup>, based on the empirical formula of grain1 (see below) and the cell volume obtained from single crystal X-ray diffraction. Metaheimite is optically biaxial. The calculated average refractive index  $n_{av}(calc)=1.894$  is based on an ideal formula with three hydrogen atoms. Based on the empirical formula for grain 1,  $n_{av}(calc)=1.885$ . The a:b:c ratios calculated from the single crystal unit-cell parameters are 0.753:1:1.792.

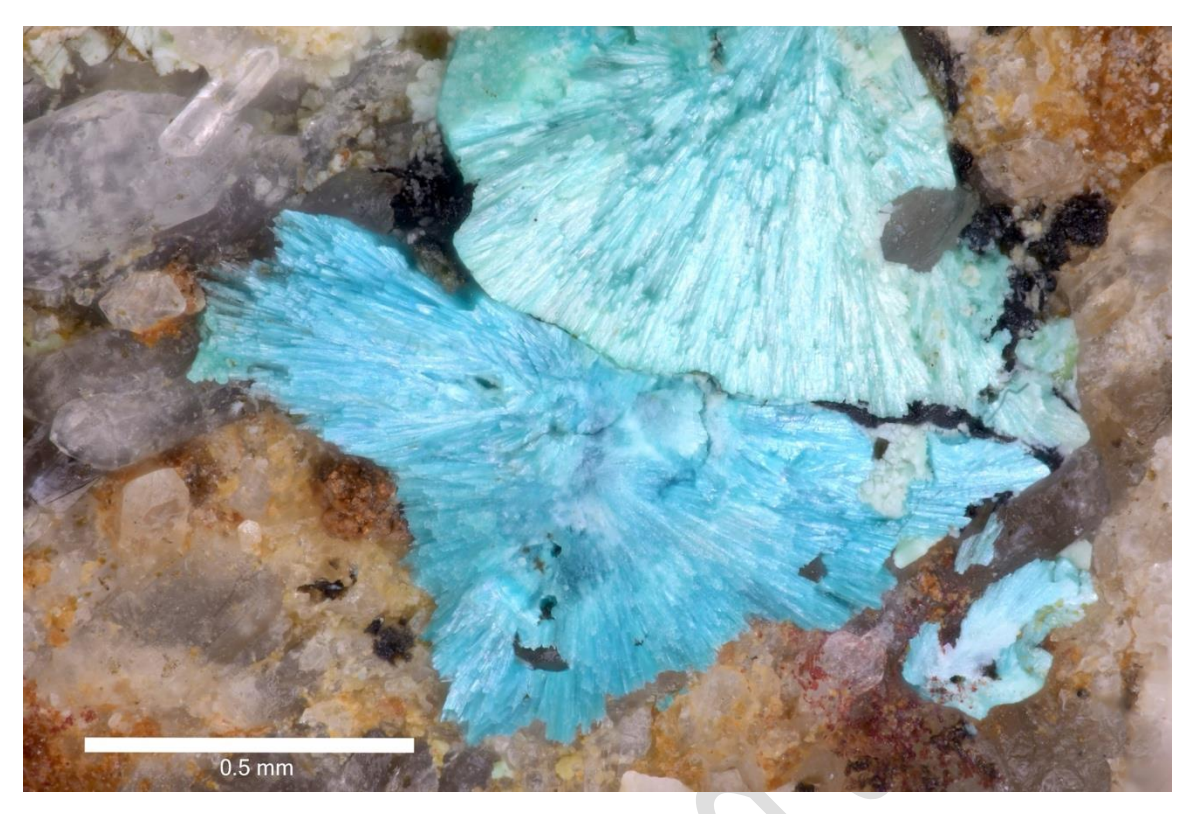


Figure 1: Sheafs of radially grown metaheimite.

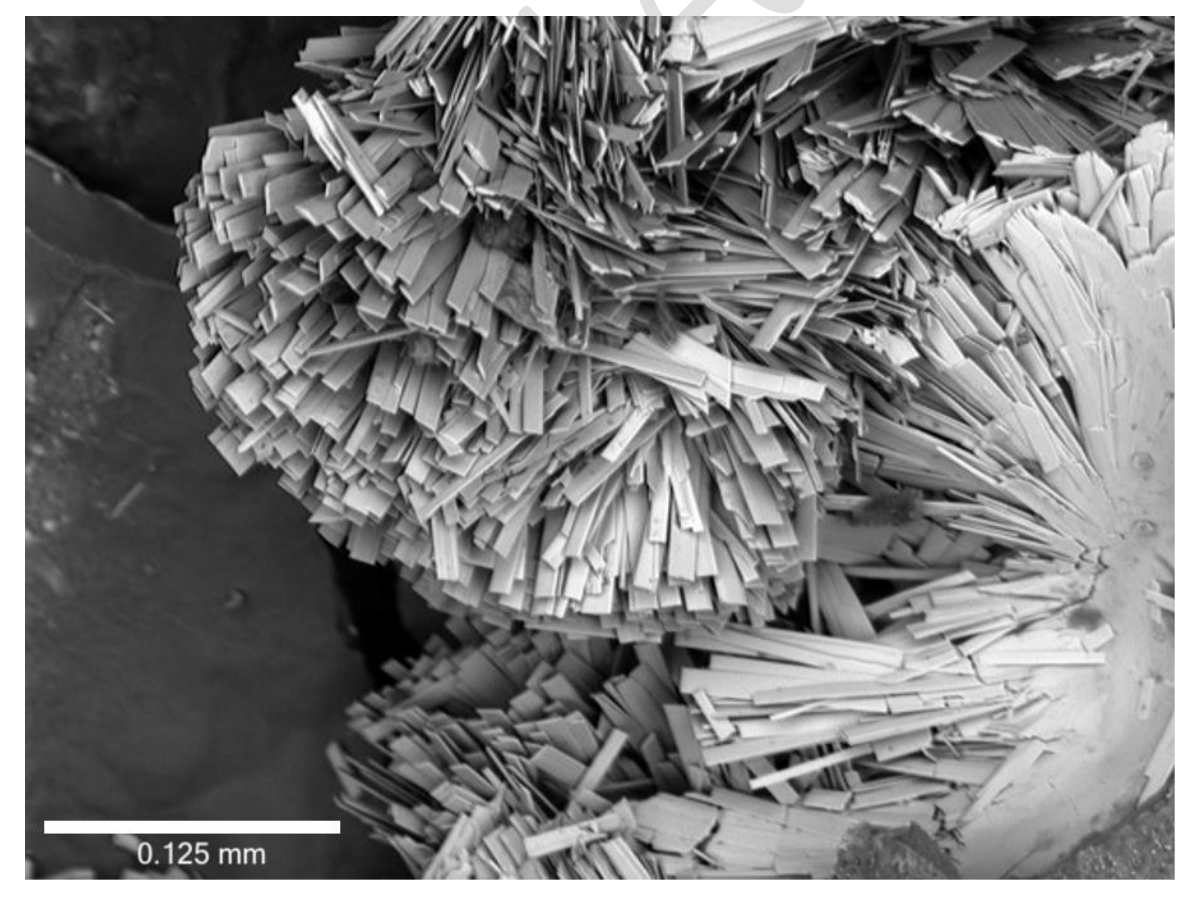


Figure 2: Scanning Electron Microscope (SEM) image of metaheimite.

## **Experimental details**

# Infrared spectroscopy

Fourier transform infrared (FTIR) spectra of heimite and metaheimite were measured in a transmission mode from single-crystal specimens that had been previously analysed by XRD, using a Bruker Invenio FTIR spectrometer equipped with a Hyperion 2000 microscope and LN2-cooled MCT detector. The crystals, approximately 0.01 mm thick, were deposited on a KBr window and oriented with (001) perpendicular to the IR beam. Spectra in the range 620 – 7000 cm<sup>-1</sup> were collected with a 15× objective, scanner velocity 20.0 kHz, an instrumental spectral resolution of 2 cm<sup>-1</sup> and averaged over 512 scans. The as-measured spectra were corrected only for the contribution from atmospheric H<sub>2</sub>O and CO<sub>2</sub>, using the corresponding option implemented in the OPUS software package. The lateral beam size was restricted by a rectangular aperture that equals the respective size of the crystal. Resolved 1<sup>st</sup>-order IR absorption signals of metaheimite occur at 673, 773, 837, 1015, 1090, 2851, 2925, 3450 and 3612 cm<sup>-1</sup>.

## Raman Spectroscopy

The same single crystals of heimite and metaheimite were further subjected to polarized Raman spectroscopy in back-scattering experimental geometry, using a Horiba Jobin-Yvon T64000 triple-monochromator spectrometer equipped with an Olympus BX41 microscope and an LN2-cooled Symphony CCD detector. For measurements in  $\bar{z}(xx)z$ ,  $\bar{z}(yy)z$ , and  $\bar{z}(yx)z$  geometries with  $x \parallel a$ ,  $z \parallel c$ ,  $y \perp$  to x and z, crystals were placed on gold wafers on their (001) face (experimental geometry given in Porto's notations,  $\mathbf{k}_i(\mathbf{E}_i\mathbf{E}_s)\mathbf{k}_s$ , in which  $\mathbf{k}_i$  and  $\mathbf{k}_s$  are the wave vectors of incident and scattered light, while  $\mathbf{E}_i$  and  $\mathbf{E}_s$  are the polarization vectors of incident and scattered light, Damen et al. (1966)), Measurements in  $\bar{y}(zz)y$  and  $\bar{y}(xz)y$  geometries were performed on crystals glued to a glass fiber, so that [001] could be oriented normal to the incident light. The spectra were excited with the green line ( $\lambda$  = 514.532 nm) of an Ar<sup>+</sup> laser (Coherent Innova 90C FreD). In order to prevent sample overheating during the measurements, a low laser power of 735  $\mu$ W on the sample surface and laser-spot diameter of 2  $\mu$ m was used. The instrumental accuracy in determining the peak position was ~0.35 cm<sup>-1</sup>, while the spectral resolution was ~1.9 cm<sup>-1</sup>. The as-measured spectra

were baseline corrected for the weak continuum photoluminescence background, using a spline interpolation, and then temperature reduced, to account for the Bose-Einstein distribution of phonons. The range 2600 – 3800 cm<sup>-1</sup> of the Raman spectra, generated by stretching modes of OH<sup>-</sup> and H<sub>2</sub>O, was fitted with pseudo-Voigt functions to determine the peak positions, full widths at half maximum and relative intensities. Additional Raman spectra were collected from several spatial points to verify the repeatability of the data. Test measurements conducted with the 488.0-nm laser line confirmed that all observed peaks in the range 15 - 3300 cm<sup>-1</sup> are Raman-scattering signals, i.e. originate from inelastic light scattering by atomic vibrations, and none are sharp photoluminescence signals from plausible impurities of ppm concentrations.

## Electron microprobe analysis

Two small grains of metaheimite were embedded in epoxy and carbon coated. Small size and brittleness of the crystals prevented the sample surface from being perfectly planar and crack free, which may account for slightly low oxide sums. Wavelength dispersive spectra were measured using a Cameca SX 100 with 15 kV, 20 nA and a beam diameter of approximately 5 μm. H<sub>2</sub>O was not directly determined due to the small amount of material available, but the presence of OH-groups and the absence of significant molecular H<sub>2</sub>O is confirmed by infrared and Raman spectroscopy. H<sub>2</sub>O content estimated by difference to 100% was included in the ZAF matrix correction. Wollastonite (34.5 Ca, 24.18 Si, 41.32 O), olivenite (44.91 Cu, 0.36 H, 26.47 As, 28.26 O) and a Pb-glass (51.63 Pb, 13.52 Si, 0.16 Al, 0.05 Fe, 0.05 Mg, 11.2 Zn, 0.02 Na, 0.02 K, 22.36 O) were used as standards (compositions in wt%).

# X-ray diffraction

Single-crystal and powder XRD studies were carried out using a Nonius KappaCCD single crystal diffractometer with graphite monochromated  $MoK\alpha$  radiation ( $\lambda = 0.71075$  Å). Pixel integration and data reduction were performed with the Eval15 program suite (Schreurs et al., 2010). A numerical absorption correction based on crystal morphology was calculated using Sadabs (SADABS-2008/1).

Powder XRD data were collected using Gandolfi-type motion of a polycrystalline aggregate of metaheimite mounted on a glass fiber at 60 mm detector distance. Powder rings up to  $2\theta = 30^{\circ}$  were integrated using the program Fit2d (Hammersley, 2016). Unit cell parameters were

obtained by Rietveld refinement, with all atomic parameters and the  $\beta$ -angle fixed at values obtained by single crystal XRD. Appropriate profile parameters were obtained by LeBail refinement of a similarly measured Si powder standard.

## Results

## Chemical composition

Results of electron microprobe analyses of metaheimite are reported in Table 1.

Table 1. Chemical composition of metaheimite in oxides (wt%).

		Grain1		Grain2			
Oxide	Mean	Range (5 pnts)	Stand. Dev.	Mean	Range (4 pnts)	Stand. Dev.	Probe Standard
CuO	29.96	26.06-31.74	2.03	29.51	29.06-30.00	0.36	Cu $K\alpha$ , olivenite
PbO	40.85	38.18-43.18	1.63	41.38	40.70-41.87	0.45	Pb Mα, Pb-glass
CaO	0.30	0.05-1.21	0.45	0.05	0.03-0.06	0.01	Ca <i>K</i> α, wollastonite
$As_2O_5$	22.10	19.49-24.41	1.91	21.53	21.31-21.80	0.18	As $L\alpha$ , olivenite
H <sub>2</sub> O <sub>calc</sub>	5.13*			5.03*			
Total	98.34			97.50			

<sup>\*</sup>H<sub>2</sub>O<sub>calc</sub> based on structure refinement with 3 H atoms.

Assuming 3 H atoms and normalizing to 7 anions, empirical formulas of  $(Pb_{0.96}Ca_{0.03})_{\Sigma 0.99}Cu_{1.98}(As_{1.01}O_4)(OH)_3$  and  $Pb_{0.99}Cu_{1.99}(AsO_4)(OH)_3$  can be obtained for grain 1 and grain 2 respectively. The simplified formula of metaheimite is  $(Pb,Ca)Cu_2(AsO_4)(OH)_3$ . The ideal formula is  $PbCu_2(AsO_4)(OH)_3$ , which requires CuO 30.36, PbO 42.56,  $As_2O_5 21.93$ ,  $H_2O 5.15$ , total 100 wt%.

The results of the XRD measurements are summarized in Table 2.

Powder XRD data for metaheimite are compiled in Table 3. The values  $d_{\rm calc}$  and  $I_{\rm calc}$  have been calculated from single-crystal diffraction data using the program JANA2006 (Petříček et al., 2014). Peak positions  $d_{\rm meas}$  and intensities,  $I_{\rm meas}$ , have been obtained using Gaussian profile fitting of the observed powder diffraction profile. Only those lines with calculated relative intensity  $I_{\rm calc} > 15\%$  are included in Table 3.  $I_{norm}$  has been normalized to the sum of

overlapping reflection intensities  $I_{\text{calc}}$ , providing a better match for the intensities  $I_{\text{meas}}$  of the observed, broad reflections in the powder diffraction profile.

Table 2. Crystal properties of metaheimite.

	single crystal	crystal aggregate	
Crystal system	monoclinic	orthorhombic	monoclinic
Space group	P2 <sub>1</sub> /n (#14)	Pnma (#62)	$P2_{1}/n (#14)$
Z	4	1 mma (1102)	12/11 (111)
$\lambda$ (Å)	0.71075		
a (Å)	5.8347(4)	7.7528(6)	5.816(4)
b (Å)	7.7528(6)	5.8347(4)	7.738(7)
c (Å)	13.8899(9)	13.8899(9)	13.912(11)
β (°)	90.018(3)	90	90.018
$V(\mathring{A}^3)$	628.31(8)	628.31(8)	626.1(6)
μ (mm <sup>-1</sup> )	38.7		
ρ (g cm <sup>-3</sup> )*	5.54		
F(000)	928		
obs criterion	$I > 3\sigma(I)$		
$\theta_{\min}, \theta_{\max}(^{\circ})$	2.8, 30		1.5, 15
Crystal size (mm)	0.1 x 0.02 x 0.01		
hkl ranges	-8, 8, -10, 10, -19, 19	-10,10, -8, 8, -	
		19,19	
R <sub>int</sub>	0.0565	0.058	
Structure factor coefficient	$F^2$		
N <sub>refl.</sub> : total, unique, obs	19343, 1814, 1393	18904, 999, 831	
R <sub>obs</sub> , R <sub>all</sub>	0.0613, 0.0798	0.0622, 0.0734	
wR <sub>obs</sub> , wR <sub>all</sub> **	0.151, 0.157	0.154, 0.158	
GoF	2.03	2.25	
N <sub>parameters</sub>	106	65	
N <sub>restraints</sub> , N <sub>constraints</sub>	2, 6	2, 5	
$\Delta \rho_{\text{max}}$ , $\Delta \rho_{\text{min}}$ (e Å <sup>-3</sup> )	9.50, -2.79	9.91, -2.51	

<sup>\*</sup>Density based on ideal formula, PbCu<sub>2</sub>(AsO<sub>4</sub>)(OH)<sub>3</sub>

<sup>\*\*</sup>Weighting scheme  $w = 1/(\sigma^2(I) + 0.025 I^2)$ 

Table 3. X-ray powder diffraction data (d in Å) for metaheimite. The seven strongest calculated lines are given in bold.

I <sub>meas</sub>	$d_{meas}$	$d_{calc}$	h	k	l	$I_{calc}$	$I_{ m norm}$	
43	7.070	6.945	0	0	2	100	26	
0		6.770	0	1	1	18	5	
	7 OF 6	5.380	-1	0	1	49		
18	5.376	5.379	1	0	1	50	25	
3	5.105	5.173	0	1	2	34	9	
		3.975	0	1	3	73	-	
	• 0 • •	3.876	0	2	0	26	- 4	
67	3.863	3.871	-1	1	2	75	64	
		3.870	1	1	2	75		
0		3.734	0	2	1	26	7	
0		3.472	0	0	4	25	6	
-		3.385	0	2	2	41		
		3.286	-1	1	3	27		
36	3.240	3.285	1	1	3	27	30	
		3.229	1	2	0	22		
		3.169	0	1	4	78		
100	3.139	3.145	4	2	1	99	71	
100	0.105	3.145	1	2	1	99	, -	
		2.972	0	2	3	60		
		2.928	-1	2	2	24		
38	2.926	2.928	1	2	2	24	40	
		2.917	2	0	0	50		
		2.785	-1	1	4	73		
37	2.778	2.785	1	1	4	73	37	
	2.673	2.690	-2	0	2	47		
		2.689	2	0	2	47		
59		2.679	-2	1	1	46	48	
		2.679	2	1	1	46		
		2.649	-1	2	3	36		
21	2.615	2.648	1	2	3	36	39	
21	2.013	2.615	0	1	5	81	39	
		2.586	0	2	4	26		
		2.541	-2	1	2	51		
41	2.546	2.541	2	1	2	51	44	
		2.541	0	3	1	45		
		2.352	-2	1	3	43		
21	2 224	2.352			3		34	
21	2.334	2.332	2 2	2	0	41 50	34	
		2.299	-2	2	1	17		
		2.299	2	2	1	17		
		2.257	0	3	3	55		
20	2.248	2.237	-1	3	2	27	52	
20	2.248	2.237	1	3	2	26	32	
		2.237	-2	2	2	31		
			2	2		31		
		2.210			2			
		2.106 2.106	-1 1	2 2	5	20 20		
			-1	3	3			
		2.105				21	1	
17	2.082	2.105	1	3	3	21	57	
		2.082	-2	2	3	34		
		2.082	2	2	3	34		
		2.074	-1	1	6	37	_	
		2.073	1	1	6	36		

0		1.988	0	2	6	34	9	
U		1.954	-1	3	4	30	9	
		1.953	1	3	4	30		
		1.948	-2	1	5	17		
		1.947	2	1	5	16		
13	1.938	1.938	0	4	0	19	43	
		1.926	-3	0	1	16		
		1.926	3	0	1	16		
		1.920	0	4	1	26		
0		1.892	0	3	5	25	6	
		1.879	-1	0	7	19		
		1.878	1	0	7	19		
13	1.864	1.867	0	4	2	41	29	
		1.864	-2	3	2	18		
		1.863	2	3	2	18		
		1.823	-1	4	1	27		
		1.823	1	4	1	27		
		1.821	-3	1	2	27		
		1.820	3	1	2	27		
		1.814	-2	0	6	44		
25	1.810	1.813	2	0	6	44	83	
		1.800	-1	3	5	17		
		1.800	1	3	5	17		
		1.788	0	4	3	23		
		1.785	-2	3	3	36		
		1.785	2	3	3	36		
	1.724	1.736	0	0	8	29		
26		1.725	-3	2	1	41	477	
26	1.724	1.725	3	2	7	41	47	
		1.691	-1 1	2 2	7	37 37		
		1.658	-3	1	4	35		
		1.657	3	1	4	35		
		1.628	-3	2	3	17		
		1.627	3	2	3	16		
		1.614	2	4	0	56		
		1.605	-2	1	7	18		
44	1.609	1.605	2	1	7	18	100	
		1.604	-2	4	1	21		
		1.604	2	4	1	21		
		1.588	-2	3	5	55		
		1.587	2	3	5	55		
		1.585	0	2	8	16		
		1.574	0	3	7	28		
		1.514	0	1	9	16		
5	1.506	1.513	0	5	2	25	20	
5	1.500	1.492	-2	0	8	20	20	
		1.492	2	0	8	20		
		1.486	0	4	6	35		
		1.465	-2	1	8	21		
		1.465	2	1	8	21	55	
14	1.474	1.465	-1	5	2	24		
-		1.465	1	5	2	24		
		1.463	-3	1	6	21		
		1.462	3	1	6	21		
		1.459	4	0	0	48		

## **Crystal structure**

The crystal of metaheimite used for this study was a blade extending along [100], about 0.1 mm long, 0.01 mm thick and 0.02 mm wide. It consists of at least three fragments, each tilted by about 9° around approximately the direction of crystal elongation. The main domain accounts for 64% of the crystal volume. The structure was solved using Superflip (Palatinus & Chapuis 2007) and refined using JANA2006 based on 19343 non-overlapping reflections of the main domain, averaged to 1814 unique reflections. Scattering factors of the uncharged atoms were used for the refinement, which converged to  $R_{obs}$  = 6.1%, with the largest residual electron density  $\Delta \rho_{max}$  (Table 2) occurring at 1.39 Å distance from the position of the Pb atom. Likely causes of this and other residual maxima as well as the high R-factor are absorption artifacts and crystal fragmentation.

The crystal structure of metaheimite is closely related to that of heimite (Malcherek *et al.* 2024). It results from different stacking of structural layers similar to those observed in heimite. Unit cell parameters and selected *d*-spacings of the two minerals are compared in Table 4.

Table 4. Cell parameters and calculated positions of strong powder diffraction lines of heimite compared to those of metaheimite.

	metaheimite	heimite
a (Å)	5.8347(4)	5.9132(5)
b (Å)	7.7528(6)	7.8478(6)
c (Å)	13.8899(9)	16.8158(15)
β (°)	90.018(3)	90.007(6)
$V(\text{Å}^3)$	628.31(8)	780.33(8)
$d_{002}(A)$	6.945	8.425
$d_{112}(A)$	3.870	4.143
$d_{014}(A)$	3.169	3.713
$d_{120}(A)$	3.229	3.276
$d_{121}$ (Å)	3.145	3.216
$d_{023}$ (Å)	2.972	3.221

The two crystal structures in projection along [100] are compared in Figure 3. Crystal structure drawings have been prepared using CrystalMaker X (Palmer 2015). As no molecular  $H_2O$  could be located in metaheimite,  $Cu^{2+}$  is only [4+1], rather than [4+2]-coordinated as in heimite (Malcherek et al. 2024), forming tetragonally elongated and edge-sharing  $CuO_5$ -square pyramids (Figure 4a), with their tips pointing along [011] and [011]. The resulting

[100] chains of square pyramids are laterally connected by  $AsO_4$ -tetrahedra and by [6+2]-coordinated  $Pb^{2+}$ -cations (Figure 4b), thus forming layers parallel to (001). These layers are mutually connected by hydrogen bonding (Table 5).

Table 5. Hydrogen bonding of metaheimite. Calculated O-H stretching frequencies (Libowitzky 1999) are given in the final column (D = Donor, A = Acceptor).

Donor	Hydr	Accep	D-H	HA	D-A	A-HD	Frequency
	ogen	tor	distance	distance	distance	angle	(cm <sup>-1</sup> )
			(Å)	(Å)	(Å)	(°)	
O4	H4	O5	0.96(12)	2.22(12)	3.099(15)	152(11)	3572
O6	Н6	O5	1.0	1.62	2.590(14)	162.2	2663
O7	H7	O4	1.02(10)	1.97(12)	2.917(15)	153(10)	3513

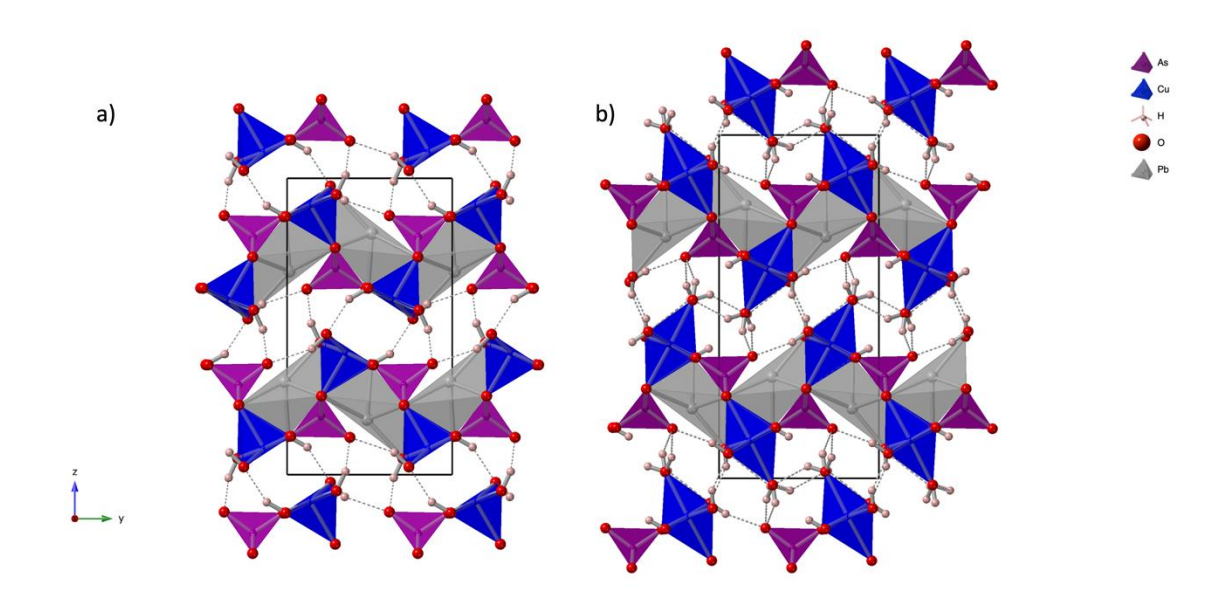


Figure 3. Crystal structure of metaheimite (a) and of heimite (b) in projection along [100]. Dashed lines indicate hydrogen bonding.

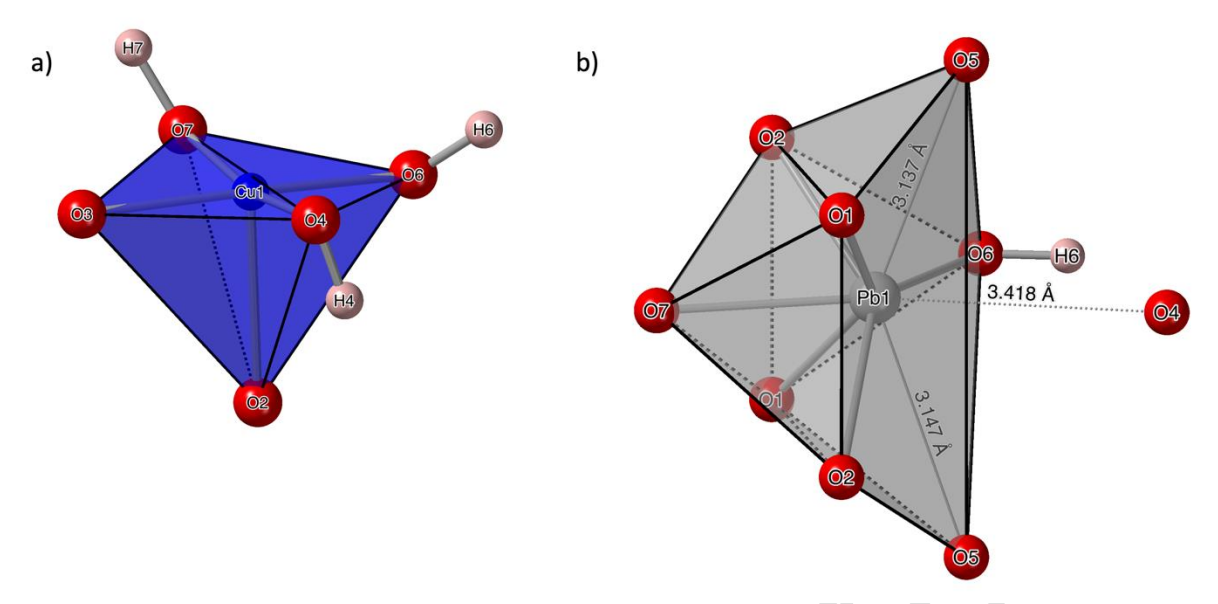


Figure 4. Square-pyramidal Cu-coordination polyhedron (a) and [6+2] Pb-coordination (b), also showing the more distant O4 anion.

Each Cu<sup>2+</sup> cation shares two of its oxygen ligands with neighbouring As<sup>5+</sup> cations. The remaining oxygen ligands form OH-groups. Positions of hydrogen atoms were either obtained from difference Fourier maxima (atoms H4, H7) or inferred from tetrahedral coordination of the donor oxygen atom (atom H6). Bond length restraints (O4-H4, O7-H7) and constraints (O6-H6) of 1 Å were imposed for the OH-groups and isotropic H displacement factors were coupled to the donor oxygen displacements by a factor of 1.2.

As can be seen in Figure 3, the absence of interlayer  $H_2O$  molecules in metaheimite requires the layers to shift relative to each other, resulting in a different hydrogen bonding scheme compared to heimite and in smaller Cu-Cu distances between adjacent layers (Figure 3). The layer-shift manifests itself by a change in the *y*-coordinate of approximately -1/3 for all atoms relative to their positions in the heimite structure (Table 6). The smaller interlayer spacing and lack of water molecules are responsible for the significantly smaller c unit-cell parameter of metaheimite in comparison to heimite (Table 4).

Anisotropic displacement factors are given in Table 7. Some of the oxygen atoms, O7 in particular, exhibit very small  $U^{11}$  displacement factors, which are attributed to absorption effects. The displacement factors remain almost identical in the orthorhombic structure model.

Table 6. Atomic positions and equivalent isotropic displacement factors,  $U_{eq}$ , of metaheimite. Corresponding parameters for heimite are given below each line.

Atom	X	y	z	$U_{\rm eq}({\rm \AA}^2)$
Pb1	0.24999(10)	0.48553(7)	0.18609(4)	0.01946(18)
	0.25001(4)	0.83278(3)	0.203979(13)	0.0122(4)
As1	0.7499(2)	0.70644(18)	0.30278(10)	0.0121(4)
	0.74997(8)	0.03728(7)	0.29566(3)	0.00899(14)
Cu1	0.9982(3)	0.3602(2)	0.41110(12)	0.0145(5)
	0.99850(11)	0.69637(9)	0.38968(4)	0.01234(18)
Cu2	0.5018(3)	0.3600(2)	0.41115(12)	0.0144(5)
	0.50146(11)	0.69643(9)	0.38971(4)	0.01218(18)
O1	0.9870(17)	0.7081(13)	0.2346(7)	0.019(3)
	0.9875(6)	0.0450(5)	0.2394(2)	0.0145(11)
O2	0.5134(16)	0.7080(13)	0.2343(7)	0.019(3)
	0.5139(6)	0.0455(5)	0.2394(2)	0.0141(11)
O3	0.7490(17)	0.5230(12)	0.3703(8)	0.014(3)
	0.7504(6)	0.8568(5)	0.3517(3)	0.0134(10)
O4	0.7494(16)	0.2386(14)	0.4738(7)	0.017(3)
	0.7491(7)	0.5581(5)	0.4277(2)	0.0127(10)
O5	0.751(2)	0.8804(14)	0.3740(7)	0.027(4)
	0.7502(8)	0.2091(5)	0.3553(3)	0.0222(12)
O6	0.2504(16)	0.7013(11)	0.0548(7)	0.013(3)
	0.2496(6)	0.0389(5)	0.0873(2)	0.0144(11)
O7	0.2499(17)	0.5085(12)	0.3709(8)	0.013(3)
	0.2502(7)	0.8364(5)	0.3522(3)	0.0142(11)
H4	0.77(3)	0.151(15)	0.425(9)	0.0199
	0.740(12)	0.459(7)	0.397(4)	0.0152
Н6	0.2508	0.6464	-0.0103	0.0159
	0.236(13)	0.044(9)	0.035(3)	0.0173
H7	0.25(3)	0.623(10)	0.407(10)	0.0199
	0.231(12)	0.936(7)	0.378(4)	0.0171

Table 7. Anisotropic displacement factors of metaheimite in  $\mathring{A}^2$ .

Atom	$U^{11}$	$U^{22}$	$U^{33}$	$U^{12}$	$U^{13}$	$U^{23}$
Pb1	0.0149(3)	0.0181(3)	0.0254(3)	0.0000(2)	-0.0001(2)	0.0015(2)
As1	0.0046(6)	0.0125(7)	0.0193(7)	0.0003(5)	0.0001(5)	0.0016(5)
Cu1	0.0032(7)	0.0164(9)	0.0236(9)	0.0005(6)	0.0006(6)	0.0024(6)
Cu2	0.0030(7)	0.0169(9)	0.0231(9)	-0.0005(6)	-0.0001(6)	0.0027(6)
O1	0.009(5)	0.018(5)	0.029(6)	0.000(4)	0.002(4)	0.008(4)
O2	0.003(4)	0.022(9)	0.030(6)	0.000(4)	-0.001(4)	0.008(4)
O3	0.005(4)	0.017(5)	0.020(5)	0.000(4)	0.000(4)	0.004(4)
O4	0.003(4)	0.026(6)	0.021(5)	0.000(4)	0.001(4)	-0.002(4)
O5	0.051(8)	0.023(6)	0.008(5)	-0.001(6)	-0.001(5)	-0.002(4)
O6	0.005(4)	0.013(5)	0.022(5)	-0.001(3)	0.000(3)	-0.005(4)
O7	0.001(4)	0.021(5)	0.027(6)	0.001(4)	0.001(4)	0.012(4)

Selected bond distances are shown in Table 8. The closest oxygen atom in a neighbouring layer that could serve to complete the Cu coordination to a [4+1+1] coordination is O3 at 3.49 Å distance. This is further than the distance to the nearest Cu-atom (3.29 Å) in that same layer. Similar to heimite, intrachain Cu-Cu distances amount to 2.9 Å on average. The mean Cu-O bond lengths (Table 8) are in good agreement with the grand mean value of 2.040 Å reported by Eby & Hawthorne (1990) for square pyramidal Cu coordination observed in nine different mineral species.

Table 8. Selected bond distances in Å.

Pb1-O1	2.407(10)	Cu1-O2	2.340(10)
Pb1-O2	2.407(10)	Cu1-O3	2.007(10)
Pb1-O6	2.474(9)	Cu1-O4	1.941(10)
Pb1-O7	2.574(11)	Cu1-O6	1.973(9)
Pb1-O1	2.863(10)	Cu1-O7	1.947(10)
Pb1-O2	2.865(10)	<cu1-o></cu1-o>	2.042
<pb-o></pb-o>	2.598	Cu2-O1	2.341(10)
Pb1-O5	3.148(13)	Cu2-O3	1.998(10)
Pb1-O5	3.135(13)	Cu2-O4	1.935(10)
As1-O1	1.677(10)	Cu2-O6	1.976(9)
As1-O2	1.675(10)	Cu2-O7	1.948(10)
As1-O3	1.705(11)	<cu2-o></cu2-o>	2.040
As1-O5	1.672(11)		
<as-o></as-o>	1.682		

The presence of hydrogen bonds is confirmed by the infrared absorption spectrum (Figure 5) and by polarized Raman spectra (Figure 6). Due to the difference in the thickness of measured specimens, the IR spectrum of heimite presented in Figure 5 is of better quality than that previously published (Malcherek *et al.* 2024). The comparison with the metaheimite IR spectrum clearly demonstrates the presence of H<sub>2</sub>O in heimite by much stronger IR absorption in the range 3100-3230 cm<sup>-1</sup> and near 1580 cm<sup>-1</sup>, corresponding to water stretching and bending modes respectively.

The sharp OH-stretching peak at 3612 cm<sup>-1</sup> is close to that observed at 3602 cm<sup>-1</sup> in heimite (Figure 5). The corresponding Raman signals (Figure 6) occur at 3612.7(3) cm<sup>-1</sup> and 3602(2) cm<sup>-1</sup> respectively, but the Raman intensity is much weaker in metaheimite compared to heimite. For both minerals the intensity of this OH-stretching mode is stronger in  $\bar{z}(yy)z$  and  $\bar{y}(zz)y$  than in  $\bar{z}(xx)z$  spectra, indicating that the hydroxyl bonds generating this mode are oriented predominantly to be within the (100) plane. Considering the longest hydrogen

bond O4-O5 (Table 5) and the O4-H4 bond orientation from structure refinement, the 3612 cm<sup>-1</sup> signal is assigned to O4-H4 stretching in metaheimite, while the assignment of the 3602 cm<sup>-1</sup> signal to O7-H7 bond stretching in heimite is confirmed. Figure 7 shows details in the range between 2600 and 3800 cm<sup>-1</sup>, with peaks fitted to the Raman signals in the  $\bar{y}(zz)y$  spectra of heimite and metaheimite.

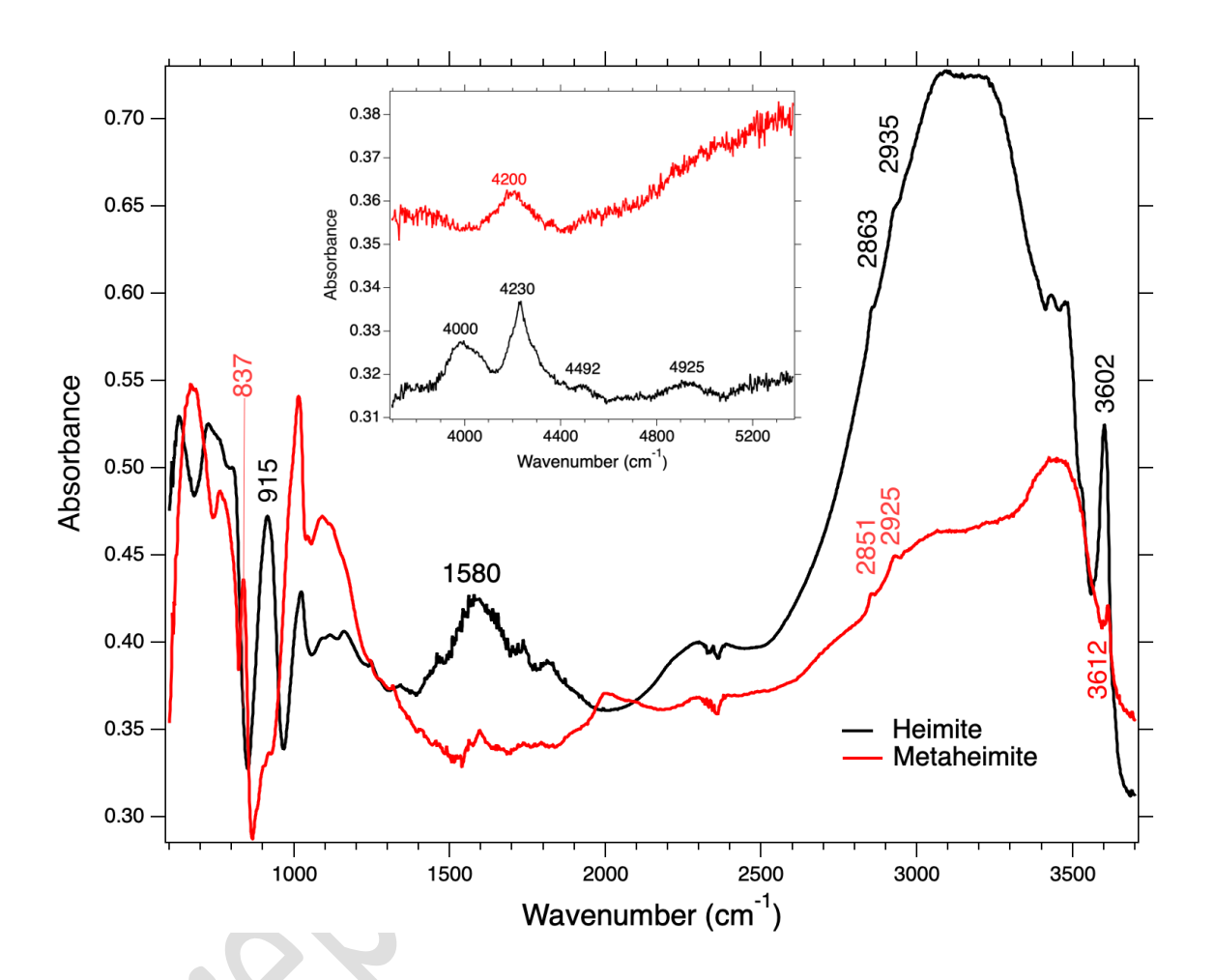


Figure 5. Infrared absorption spectrum of metaheimite (red) and heimite (black). The inset shows the near infrared range between 3800 and 5500 cm<sup>-1</sup>, generated by combinational modes of hydrous species.

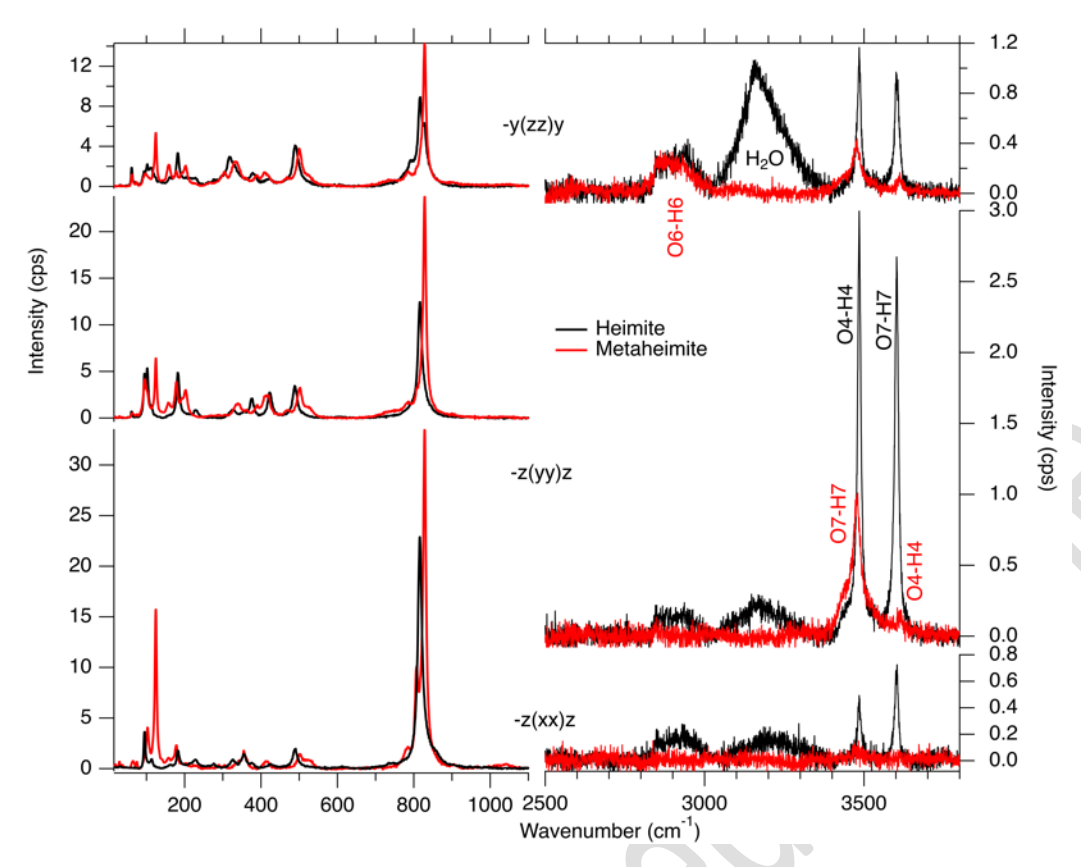


Figure 6. Parallel polarized Raman spectra of metaheimite (red) and of heimite (black) with the incident-light polarization parallel to [100]  $(\bar{z}(xx)z)$ , [010]  $(\bar{z}(yy)z)$  and [001]  $(\bar{y}(zz)y)$ .

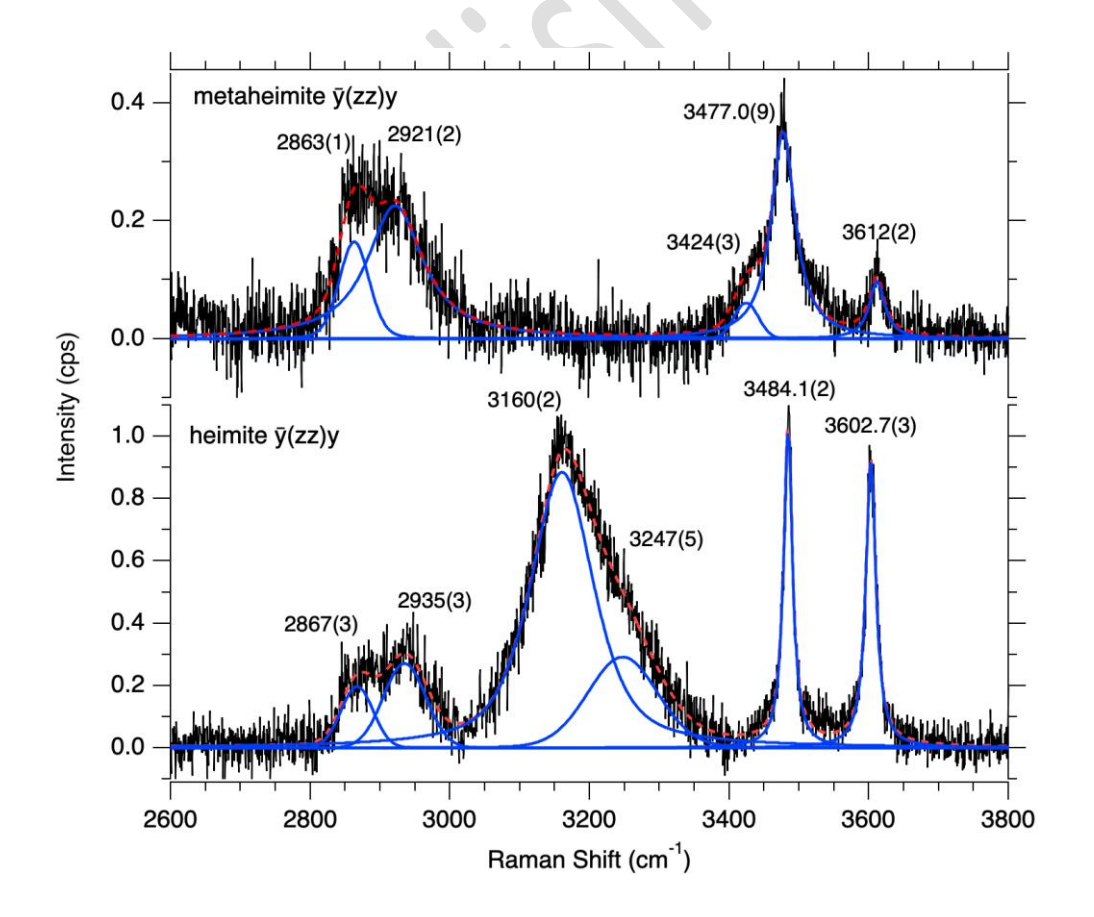


Figure 7: Enlarged and peak deconvoluted section of the  $\bar{y}(zz)y$  Raman spectra of metaheimite (top) and of heimite (bottom).

The Raman spectra of heimite in Figure 6 show another very sharp OH-stretching mode at 3484.1(2) cm<sup>-1</sup>. This can be assigned to O4-H4 bond stretching. In metaheimite, a comparable, but broader signal appears at 3477 cm<sup>-1</sup>. This is assigned to O7-H7 bond stretching, with an O7-O4 hydrogen bond length of 2.917 Å (Table 5). Both Raman signals in heimite as well as in metaheimite have shoulders at their low frequency side, most evident in the  $\bar{z}(yy)z$  spectrum. The relative intensity of this shoulder is higher in metaheimite, where it can also be observed in the  $\bar{y}(zz)y$  spectrum at 3424(3) cm<sup>-1</sup> (Figure 6). It may be attributable to static or dynamic H-disorder along the chain of hydrogen bonds O5—H4-O4—H7-O7. Only heimite shows a broad H<sub>2</sub>O stretching signal in the frequency range 3020 - 3400 cm<sup>-1</sup> (Figure 6). The signal is most prominent in the  $\bar{y}(zz)y$  polarized spectrum and consists of a stronger peak at 3160(2) and a weaker peak at 3247(5) cm<sup>-1</sup> (Figure 7), related to the stretching modes of H<sub>2</sub>O. The absence of this signal in metaheimite clearly indicates the absence of H<sub>2</sub>O molecules in this mineral.

Between 2820 and 3010 cm<sup>-1</sup> another broad signal is evident in the Raman spectra of both heimite and metaheimite. In metaheimite this can be decomposed into two broad peaks located at 2863(1) and 2921(2) cm<sup>-1</sup>, while in heimite the respective peaks are located at 2867(3) and 2935(3) cm<sup>-1</sup> (Figure 6). While this doublet is present in all three parallel polarized spectra  $\bar{z}(xx)z$ ,  $\bar{z}(yy)z$  and  $\bar{y}(zz)y$  for heimite, it is only present in the  $\bar{y}(zz)y$  spectrum for metaheimite (Figure 6), indicating nearly perfect orientation of the corresponding hydrogen bond along [001] in the latter. Comparing with Table 5, these signals would best match the O6-H6 bond stretching. In heimite, O6-H6 participates in significantly longer, but similarly aligned hydrogen bonds with O4 instead, while similarly short hydrogen bonds (2.68 Å) towards O5 would involve the water molecules. The reason for the similar splitting of this O-H bond stretching signal by about 60 cm<sup>-1</sup> in both minerals is not fully understood. A possible explanation may be anharmonic oscillation or splitting of the O5 ligand of the AsO<sub>4</sub> tetrahedron. The relatively large  $U^{11}$  adp parameter (Table 7), which is similarly observed in heimite, might be indicative of this.

The above OH- and  $H_2O$  stretching modes can also be observed in the respective IR absorption spectra (Figure 5), but the details are more obvious in the polarized Raman spectra. Combination modes observed in the near infrared part of the spectra (Figure 5, inset) further support the absence of  $H_2O$  in metaheimite: in the range  $4000 - 5400 \text{ cm}^{-1}$ , only a single peak

at 4200 cm<sup>-1</sup> is observed, which originates from a combination of stretching and libration modes of hydroxyl groups (e.g. Della Ventura *et al.* 2021). In strong contrast, heimite exhibits multiple 2<sup>nd</sup>-order infrared absorption signals in the same range, indicating the co-presence of different types of hydrous species. The peak near 4230 cm<sup>-1</sup> corresponds to stretching and libration of hydroxyl groups, whereas the peaks at 3985 - 4040, ~4492 and ~4925 cm<sup>-1</sup> most probably involve fundamental modes of H<sub>2</sub>O. For example, the two-component IR band at 3985-4040 cm<sup>-1</sup> could be due to a combination of the IR-active stretching of water molecules near 3105-3232 cm<sup>-1</sup> and Raman-active AsO<sub>4</sub> stretching at 810 cm<sup>-1</sup>; note that according to group theory, for centrosymmetric crystals like heimite, 2<sup>nd</sup>-order IR activity requires a combination of one Raman-active and one IR-active mode (Della Ventura *et al.* 2021). The peaks near 4492 and 4925 cm<sup>-1</sup> could arise from combinational modes of water bending and hydroxyl stretchings or higher-order combinational modes of hydroxyl stretching and librations; the unambiguous assignment is hindered by the complexity of hydrous species existing in heimite.

The low-frequency part of the spectra in Figures 5 and 6 shows many similarities between heimite and metaheimite. An intense Raman peak at 125 cm<sup>-1</sup> is unique to metaheimite, however, with highest intensity observed in the  $\bar{z}(xx)z$  spectrum. This might be attributable to the different Cu-coordination in both minerals.

Another apparent difference in the IR spectra measured in the experimental geometry described above (the IR beam perpendicular to the natural plate-like surface) can be seen in the AsO<sub>4</sub> stretching range, as metaheimite exhibits a strong IR absorption peak at 837 cm<sup>-1</sup>, which is not observed in heimite, while the IR absorption peak at 915 cm<sup>-1</sup> in the spectrum of heimite is much weaker for metaheimite and appears as a shoulder of the IR absorption signal near 1012 cm<sup>-1</sup> (Figure 5). The strongest Raman-active phonon mode related to AsO<sub>4</sub> stretching vibration appears at 828 cm<sup>-1</sup> for metaheimite and at 816 cm<sup>-1</sup> for heimite (Figure 6).

## **Discussion**

Similarly to heimite, metaheimite is pseudo-orthorhombic with a parent symmetry of Pnma. While the monoclinic symmetry of heimite was inferred from the necessity of neighbouring  $H_2O$  molecules to be non-equivalent, these molecules are absent in metaheimite. The small metric distortion is nevertheless more pronounced than in heimite and probably caused by strong and asymmetric hydrogen bonding between the layers. Table 2 compares the

refinement results for the monoclinic and the orthorhombic structure models. The structure data of the orthorhombic refinement are made available in the cif-file. The monoclinic symmetry renders adjacent Cu atoms along the [100] chains inequivalent. At least for heimite, the monoclinic distortion is confirmed by the polarized Raman spectra (Figure 6), as in the orthorhombic structure, O-H-bonds would have to reside on mirror planes normal to the elongation direction of the crystals and O-H stretching would not be expected to have any component in this direction. As the observed Raman scattering in metaheimite is generally weaker, similar signals in its  $\bar{z}(xx)z$  spectrum are not so obvious.

Metaheimite represents a new structure type. Chemically similar minerals are heimite,  $PbCu_2(AsO_4)(OH)_3 \cdot 2H_2O$ , bayldonite,  $PbCu_3(AsO_4)_2(OH)_2$ , duftite,  $PbCu(AsO_4)(OH)$ , plumboagardite,  $(Pb,REE,Ca)Cu_6(AsO_4)_3(OH)_6 \cdot 3H_2O$  and thometzekite,  $PbCu_2(AsO_4)_2 \cdot 2H_2O$ . With the exception of heimite, the crystal structures of all these minerals differ significantly from the metaheimite structure.

Bond valence sums (BVS) at the cation positions (Table 9) agree well with their formal charges. As in heimite, O5, the "free" corner atom of the AsO<sub>4</sub> tetrahedron, is underbonded, despite its slightly shorter distance to Pb in metaheimite (3.14 Å; Table 7) compared to heimite (3.27 Å).

Table 9. Bond valences of metaheimite. Bond valence parameters are taken from Gagné & Hawthorne (2015) and from Malcherek & Schlüter (2007) (for H-O only). Values in italics represent the soft bond valences and related BVS based on the parameters of Malcherek & Schlüter (2007) with a 3.5 Å distance cut-off. Alternative, underlined values have been calculated using the H-O parameters of Gagné & Hawthorne (2015), based on only the two shortest O-H distances per hydrogen atom.

	Cu1	Cu2	As1	Pb1	H4	Н6	H7	Σ
O1		0.16	1.28	0.43	0.03		0.02	2.07
				0.15				<u>2.02</u>
O2	0.16		1.29	0.43	0.04		0.02	2.09
				0.15				2.03
О3	0.41	0.42	1.19		0.02	0.02	0.02	2.11
							0.02	2.02
							0.01	
O4	0.49	0.50			0.73	0.02	0.12	1.90
					<u>0.91</u>	0.02	0.08	1.98
						0.02		
O5			1.30	0.08	0.08	0.22		1.76
				0.08	0.05	0.19		<u>1.70</u>
O6	0.45	0.44		0.37	0.03	0.68	0.01	1.99
					0.01	0.83		2.09
O7	0.48	0.48		0.29		0.01	0.65	1.91
							<u>0.79</u>	<u>2.04</u>
Σ	1.99	2.00	5.06	1.98	0.94	0.99	0.87	
					<u>0.95</u>	<u>1.02</u>	<u>0.87</u>	

The shorter Pb-O5 distances in metaheimite indicate that the Pb atom can be considered as 6+2 coordinated, rather than 6-coordinated as in heimite. This interpretation is supported by the two bond valence contributions of 0.08 v.u. (Table 9) being just at the threshold of contributing nearest neighbour bonds, i.e. 4% of the formal valence of the central cation (Brown 2002). Together with the smaller lattice parameter c and the absence of water molecules, metaheimite can thus be considered a transitional phase between heimite and the condensation of the layers that would lead to the formation of the duftite structure, with its 8-coordinated Pb-atoms and a higher Pb/Cu ratio (Malcherek et al. 2024).

For the O-H bond distances and their related bond strengths, it has to be kept in mind in the following that they are heavily influenced by the applied constraints or restraints and may only represent a poor approximation of the true O-H distances. Bond valences associated with O-H bond pairs have been calculated based on two sets of parameters. The parameters obtained by Malcherek & Schlüter (2007),  $R_0$ =0.781 Å and B=0.56 Å, involve all H-O distances up to a cut-off distance of 3.5 Å, going beyond the nearest neighbour coordination (cf. Adams 2001). This approach appears to be particularly adequate for the calculation of H-

O bond valences, considering the small coordination number (CN) and generally asymmetric coordination of the hydrogen atom. It should be noted that in analogy to the Pb-coordination described above, only bond valences larger than 0.04 v.u. indicate nearest neighbour bonds. Hence the consideration of longer distances and smaller bond valences does not increase the CN of the hydrogen atoms beyond two for metaheimite.

The second model (underlined numbers) involves the parameters determined by Gagné & Hawthorne (2015),  $R_0$ =0.918 Å and B=0.427 Å. Here only the nearest neighbour bonds (Table 5) are considered for the calculation of the BVS.

By the results shown in Table 9 it can be concluded that the cationic BVS deviate very little between the two models. Stronger deviations occur for the anionic BVS. The BVS of O4 and O7 improve when using the newer parameters of Gagné & Hawthorne (2015). Also, the calculated overbonding is smaller for atoms O1, O2 and O3. On the other hand, this approach yields an even larger underbonding of O5 and an overbonded O6 compared to the values obtained with the parameters of Malcherek & Schlüter (2007).

The structural similarity of the layers forming the heimite and the metaheimite structure would allow for stacking of  $H_2O$ -bearing and  $H_2O$ -free layers. Interjection of few heimite-layers or layer packets into the metaheimite structure would give rise to stacking faults and would cause residual  $H_2O$  content of the metaheimite crystal bulk.

The colour variations across the two minerals may be related to their water content and the resulting changes in Cu-coordination. For heimite, green, but also faint blue colours have been observed (Malcherek et al. 2024). Blue colour of heimite has also been obtained for some samples exposed to the conditions in the SEM (Roth 2022). So far only blue coloured metaheimite has been observed, which would suggest that blue colour in these minerals can serve as an indicator of at least partially vacant H<sub>2</sub>O sites and the related presence of [4+1]-coordinated Cu-atoms.

## Acknowledgements

Sample preparation and microprobe analysis were kindly carried out by Peter Stutz and Stefanie Heidrich, respectively. The characterization and preservation of the mineral paragenesis of metaheimite have benefited from funding by the Swiss Academy of Sciences (SCNAT) through SwissCollNet project no. SCN201-VD to Nicolas Meisser. Comments by

Peter Leverett, Herta Effenberger and an anonymous reviewer helped to improve the manuscript.

Competing interests: The authors declare none

## **REFERENCES**

Adams S. (2001) Relationship between bond valence and bond softness of alkali halides and chalcogenides. Acta Crystallographica, B**57**, 278-287.

Bächtiger K. (1963) Die Kupfer- und Uranmineralisationen der Mürtschenalp (Kt. Glarus, Schweiz). Beiträge zur Geologie der Schweiz, Geotechnische Serie, Lieferung 38, 113 pp.

Badertscher N.P., Beaudoin G., Therrien R. and Burkhard M. (2001) Glarus overthrust: A major pathway for the escape of fluids out of the Alpine orogen. *Geology*, **30**(10), 875–878.

Biagioni C., Roth P., Reynes J., Robyr M. and Meisser N. (2024) Zaneliite, IMA 2024-061, in: CNMNC Newsletter 82, European Journal of Mineralogy, **36**, <a href="https://doi.org/10.5194/ejm-36-1005-2024">https://doi.org/10.5194/ejm-36-1005-2024</a>.

Brown I.D. (2002) *The chemical bond in Inorganic Chemistry – The Bond Valence Model*. Oxford University Press, Oxford, UK.

Damen T. C., Porto S. P. S. and Tell B. (1966) Raman Effect in Zinc Oxide, *Physical Review*, **142**, 570, <a href="https://doi.org/10.1103/PhysRev.142.570">https://doi.org/10.1103/PhysRev.142.570</a>.

Della Ventura G., Hawthorne F. C., Mihailova B. and Sodo A. (2021) Raman and FTIR Spectroscopy of Synthetic Amphiboles: I. The OH Librational Bands and the Determination of the OH-F Content of Richterites *via* Raman Spectroscopy. *The Canadian Mineralogist*, **59**, 31–41.

Eby R.K. and Hawthorne F.C. (1990) Clinoclase and the Geometry of [5]-Coordinate Cu<sup>2+</sup> in Minerals. *Acta Crystallographica*, **C46**, 2291–2294.

Gagné O.C. and Hawthorne F.C. (2015) Comprehensive derivation of bond-valence parameters for ion pairs involving oxygen. *Acta Crystallographica*, **B71**, 562–578.

Hammersley A.P. (2016) *FIT2D*: a multi-purpose data reduction, analysis and visualization program. *Journal of Applied Crystallography*, **49**, 646-652.

Letsch, D. (2014) The Glarus Double Fold: a serious scientific advance in mid nineteenth century Alpine Geology. *Swiss Journal of Geosciences*, **107**, 65–80.

Libowitzky E. (1999) Correlation of O-H stretching frequencies and O-H···O hydrogen bond lengths in minerals. *Monatshefte für Chemie*, **130**, 1047–1059.

Malcherek T. and Schlüter J. (2007)  $Cu_3MgCl_2(OH)_6$  and the bond-valence parameters of the OH—Cl bond. *Acta Crystallographica*, **B63**, 157–160.

Malcherek T., Mihailova B., Schlüter J., Roth P. and Meisser N. (2024) Heimite, PbCu<sub>2</sub>(AsO<sub>4</sub>)(OH)<sub>3</sub>·2H<sub>2</sub>O, a new mineral from the Grosses Chalttal deposit, Switzerland. *European Journal of Mineralogy*, **36**(1), 153–164.

Malcherek T., Mihailova B., Schlüter J., Roth P., Meisser N. (2025) Metaheimite, IMA 2023-020a, in: CNMNC Newsletter 83, *European Journal of Mineralogy*, **37**, <a href="https://doi.org/10.5194/ejm-37-75-2025">https://doi.org/10.5194/ejm-37-75-2025</a>.

Meisser N. (1999) Les minéraux d'altération des indices de cuivre et uranium de la Mürtschenalp (SG/GL). *Le Cristallier Suisse*, **11**(11), 489–503 (in French and German). Palmer D. (2015) Visualization and analysis of crystal structures using CrystalMaker software, *Zeitschrift für Kristallographie*, **230**, 559–572.

Palatinus L. and Chapuis G. (2007) Superflip - a computer program for the solution of crystal structures by charge flipping in arbitrary dimensions. *Journal of Applied. Crystallography*, **40**, 786-790.

Petříček V., Dušek M. and Palatinus, L. (2014) Crystallographic Computing System JANA2006: General features. *Zeitschrift für Kristallographie*, **229**, 345–352.

Pfiffner A.O. (2014) Geology of the Alps. Wiley-Blackwell, Chichester, 376 pp.

Roth P. (2022) Heimit, ein unerwartetes, weltweit neues Mineral von einer vermeintlich bescheidenen Fundstelle, *Schweizer Strahler*, **56**, 2–9 (in French and German).

Roth P., Zanelli R. and Meisser N. (2025) Nouveautés du Grosses Chalttal, Mürtschenalp. *Le Cristallier Suisse*, **59**, 2–13 (in French and German).

Schreurs A. M. M., Xian X. and Kroon-Batenburg L. M. J. (2010) EVAL15: a diffraction data integration method based on ab initio predicted profiles. *Journal of Applied. Crystallography*, **43**, 70–82.